

Spectroscopic Orbits of Subsystems in Multiple Stars. IX

ANDREI TOKOVININ¹

¹*Cerro Tololo Inter-American Observatory — NSF's NOIRLab Casilla 603, La Serena, Chile*

ABSTRACT

New spectroscopic orbits of inner subsystems in 14 hierarchies are determined from long-term monitoring with the optical echelle spectrometer, CHIRON. Their main components are nearby solar-type stars belonging to nine triple systems (HIP 3645, 14307, 36165, 79980, 103735, 103814, 104440, 105879, 109443) and five quadruples of 2+2 hierarchy (HIP 41171, 49336, 75663, 78163, and 117666). The inner periods range from 254 days to 18 yr. Inner subsystems in HIP 3645, 14313, 79979, 103735, 104440, and 105879 are resolved by speckle interferometry, and their combined spectro-interferometric orbits are derived here. Astrometric orbits of HIP 49336 Aa,Ab and HIP 117666 Aa,Ab are determined from wobble in the observed motion of the outer pairs. Comparison with three spectroscopic orbits found in the Gaia DR3 archive reveals that Gaia under-estimated the amplitudes (except for HIP 109443), while the periods match approximately. This work contributes new data on the architecture of nearby hierarchical systems, complementing their statistics.

Keywords: binaries:spectroscopic — binaries:visual

1. INTRODUCTION

Observations of spectroscopic subsystems in nearby solar-type stars are motivated by the desire to determine their periods and mass ratios, complementing statistics of hierarchies in the solar neighborhood (Tokovinin 2014). Many subsystems discovered by, e.g., Nordström et al. (2004) or by astrometric acceleration lack orbits and therefore confuse the statistics. A long-term program at the 1.5 m telescope at Cerro Tololo with the CHIRON high-resolution optical echelle spectrograph has been conducted to determine the missing periods, with the goal to reach relative completeness for periods shorter than ~ 1000 days. The results obtained so far were reported in eight papers; the last paper 8 (Tokovinin 2022) contains references to the full series. The total number of spectroscopic orbits determined throughout this program is 102. Summary and statistical analysis of this material are presented in the accompanying paper 10 (2022, submitted). The first papers resulting from this project featured short-period orbits, but longer periods became accessible as the time coverage increased. Most orbits presented here have periods longer than a year. Some of them are preliminary, lacking adequate

phase coverage, but they are still useful for statistical purposes, justifying their publication here. Six inner subsystems are wide enough to be resolved by speckle interferometry, allowing calculation of the combined spectro-interferometric orbits.

In 2022 June, the third release of the Gaia catalog (GDR3) has changed the landscape by publishing $\sim 10^5$ spectroscopic orbits and a comparable number of astrometric orbits in their non-single star catalog, NSS (Gaia Collaboration et al. 2022). However, stars with close visual companions were removed from the Gaia SB sample. Comparison of the NSS with the CHIRON orbits, presented in paper 10, shows an overlap of only about 30%, so the NSS completeness with respect to multiple stars remains low. Some NSS orbits in common with CHIRON have substantially different parameters (examples are found below). Although the NSS orbits contribute significantly to the statistics of nearby hierarchies, they do not yet replace the ground-based monitoring and do not render the CHIRON survey obsolete.

This paper is organized similarly to the previous ones. The data and methods are outlined in Section 2, where the orbital elements are also given. The hierarchical systems are discussed in Section 3. A short summary in Section 4 concludes the paper.

2. NEW SPECTROSCOPIC ORBITS

The hierarchical systems studied here are listed in Table 1. The data are collected from Simbad and GDR3 (Gaia Collaboration et al. 2021), the radial velocities (RVs) are mostly determined in this work. The first column gives the Washington Double Star (WDS, Mason et al. 2001) code based on the J2000 coordinates. The HIP and HD identifiers, spectral types, photometric and astrometric data refer either to the individual stars or to the unresolved subsystems. Parallaxes potentially biased by unresolved subsystems are marked by colons, and asterisks indicate proper motions from Brandt (2021).

2.1. Spectroscopic Observations

Observations, data reduction, and orbit calculations were described in previous papers of this series (e.g. Tokovinin 2022). To avoid repetition, only a brief outline is given here.

The spectra used here were taken with the 1.5 m telescope sited at the Cerro Tololo Inter-American Observatory (CTIO) in Chile and operated by the Small and Medium Aperture Telescopes Research System (SMARTS) Consortium.¹ Fifteen hours of observing time were allocated to this program per semester, starting from 2017B. Observations were made with the fiber-fed CHIRON optical echelle spectrograph (Tokovinin et al. 2013; Paredes et al. 2021) by the telescope operators in service mode. The spectra taken with the image slicer have a resolution of 85 000. They are reduced by the standard CHIRON pipeline. The wavelength calibration is based on the thorium-argon lamp spectra taken after each object.

The RVs are determined from Gaussian fits to the cross-correlation function (CCF) of echelle orders with the binary mask constructed from the solar spectrum, as detailed in Tokovinin (2016a). The RV errors depend on several factors such as the width and contrast of the CCF dip, blending with other dips, and signal-to-noise ratio. The rms residuals from the orbits can be as low as 0.02 km s^{-1} , but typically are between 0.1 and 0.5 km s^{-1} for the systems studied here. I assign the RV errors (hence weights) to match roughly the residuals, with larger errors for blended or noisy dips. Some blended CCFs are fitted by fixing the width or amplitude of individual components determined from other spectra with better-separated dips. Otherwise, a heav-

ily blended dip is fitted by a single Gaussian, and the resulting biased RV is assigned a large error and a low weight in the orbit fit.

The width of the CCF dip is related to the projected rotation velocity $V \sin i$, while its area depends on the spectral type, metallicity, and, for blended spectra of several stars, on the relative fluxes. Table 2 lists average parameters of the Gaussian curves fitted to the CCF dips. It gives the number of averaged measurements N (blended CCFs of double-lined binaries are ignored), the dip amplitude a , its dispersion σ , the product $a\sigma$ proportional to the dip area (hence to the relative flux), and the projected rotation velocity $V \sin i$, estimated from σ by the approximate formula given in (Tokovinin 2016a) and valid for $\sigma < 12 \text{ km s}^{-1}$. The last column indicates the presence or absence of the lithium 6708 Å line in individual components.

2.2. Orbit Calculation

The orbital elements and their errors are determined by the least-squares fits with weights inversely proportional to the adopted RV errors. The IDL code ORBIT² was used (Tokovinin 2016b). Several double-lined pairs studied here were resolved by speckle interferometry, and in such case the combined orbits are fitted jointly to the RVs and position measurements. In some triple systems, the orbits of the outer and inner subsystems are fitted jointly to the RVs and, where available, position measurements using a modification of the same code ORBIT3 (Tokovinin 2017) described by Tokovinin & Latham (2017). Both codes allow to fix some orbital elements to avoid degeneracies (e.g. for circular or face-on orbits) or to cope with insufficient data (e.g. an incomplete coverage of the outer orbit).

Table 3 gives elements of the spectroscopic orbits in standard notation. Its last column contains the masses $M \sin^3 i$ for double-lined binaries. For single-lined systems, the mass of the primary star (listed with colons) is estimated from its absolute V magnitude, and the min-

¹ <http://www.astro.yale.edu/smarts/>

² Codebase: <http://www.ctio.noirlab.edu/~atokovin/orbit/> and <https://doi.org/10.5281/zenodo.611119>

Table 1. Basic Parameters of Observed Multiple Systems

WDS	Comp.	HIP	HD	Spectral	V	$V - K_s$	μ_α^*	μ_δ	RV	ϖ^a
(J2000)				Type	(mag)	(mag)	(mas yr ⁻¹)		(km s ⁻¹)	(mas)
00467–0426	A	3645	4449	G5	7.58	2.00	24*	–261*	9.7	30.08:
	B	M4V	15.20	4.92	21	–260	...	30.51
03046–5119	A	14307	19330	F8V	7.54	1.25	88	71	20.4	18.36
	B	14313	...	K1V	8.59	1.91	85	72	20.2	18.42:
07270–3419	A	36165	59099	F6V	7.03	1.23	–305*	96*	65.4	20.32:
	B	36160	59100	G1.5V	8.19	1.59	–307	91	64.9	20.71
08240–1548	AB	41171	70904	F2/F3V	8.55	1.06	–28*	–16*	–1.4	4.94:
10043–2823	A	49336	87416	F6V	7.82	1.19	–27	–23	–13.4	10.67:
	B	8.19	...	–49	–36	–11.8	10.94:
15275–1058	A	75663	137613	G0	8.14	1.35	–62*	–36*	–56.3	7.73
	B	9.21	1.50	–61	–35	–56.8	7.78
15577–3915	A	78163	142728	G3/5V	9.04	1.54	17	7	9.4	10.49
	B	10.30	2.08	18	7	10.5	10.65
16195–3054	A	79980	146836	F5IV	5.51	1.14	82	23	0.3	22.71
	B	79979	146835	F9V	6.82	1.11	76	27	–0.9	25.53:
21012–3511	A	103735	1999918	G3V	7.66	1.61	–176	–63	61.6	22.10:
	B	17.14	1.64	–176	–67	...	22.09
21022–4300	A	103814	200011	G3IV+K0IV	6.64	1.62	71*	–112*	–33.5	11.25
	B	103819	200026	K0III	6.90	2.27	70	–111	–35.6	11.25
21094–7310	AB	104440	200525	F9.5V	5.68	1.49	445*	–330*	–11.1	46.99:
	C	13.50	6.16	433	–303	–8.3	50.6
21266–4604	A	105879	203934	F7V	7.18	1.28	29*	–112*	35.5	12.44:
	D	9.96	1.76	31	–112	35.7	13.10
22104–5158	A	109443	210236	F8V	7.63	1.32	220*	–104*	–3.8	15.33:
	B	13.25	...	225	–104	...	15.58
23518–0637	AB	117666	223688	G5V	8.73	1.69	85*	–12*	14.3	13.4:

Proper motions and parallaxes are from Gaia DR3 (Gaia Collaboration et al. 2021). Colons mark parallaxes biased by subsystems, asterisks mark PMs from Brandt (2021).

imum mass of the secondary that corresponds to the 90° inclination is derived from the orbit. Table 4, published in full electronically, provides individual RVs and residuals to orbits. The Hipparcos number of the primary star and the system identifier (components joined by comma) in the first two columns define the pair. Then follow the Julian date, the RV, its adopted error σ (blended CCF dips are assigned larger errors), and the residual to the orbit (O–C). The last column specifies to which component this RV refers ('a' for the primary, 'b' for the secondary). The RVs of some other visual components are provided, for completeness, in Table 6. It contains the HIP number, the component letter, the Julian date, and the RV. The less accurate RVs derived from blended dips are marked by colons.

The elements of visual orbits are given in Table 5. For combined spectro-interferometric orbits, it repeats common elements, but the period P and epoch T are given in Julian years rather than days. This table also contains elements of the outer visual orbits fitted jointly with the inner subsystems using ORBIT3. The positional measurements used in these orbits are published (ex-

cept the latest observations at SOAR); they are listed together with the adopted errors and residuals in Table 7.

2.3. Complementary Data

I use here astrometry and photometry from the GDR3 (Gaia Collaboration et al. 2021) and from the earlier data releases where needed. For multiple systems, the standard astrometry is compromised by acceleration and/or unresolved companions (this bias is reduced for the stars with astrometric solutions in the NSS). The RUWE parameter (Reduced Unit Weight Error) captures the excessive astrometric noise, helping to identify biased astrometry in GDR3. Most (but not all) stars with subsystems studied here have $\text{RUWE} > 2$. Uncertain Gaia parallaxes are marked by colons in Table 1. Astrometric subsystems are detected by the increased RUWE or by the difference $\Delta\mu$ between the short-term proper motion (PM) measured by Gaia and the long-term PM μ_{mean} deduced from the Gaia and Hipparcos positions Brandt (2021). For stars with a large RUWE,

Table 2. CCF Parameters

HIP	Comp.	N	a	σ	$a\sigma$	$V \sin i$	Li
				(km s ⁻¹)	(km s ⁻¹)	(km s ⁻¹)	6708Å
3645	Aa	10	0.403	3.66	1.47	2.4	N
3645	Ab	10	0.115	3.93	0.45	3.5	N
14313	Ba	8	0.297	3.99	1.19	3.8	N
14313	Bb	8	0.232	4.30	1.00	4.7	N
36165	Aa	9	0.208	5.19	1.08	7.0	N
36160	B	4	0.403	3.49	1.41	1.4	N
41171	Aa	12	0.030	18.08	0.46	32.0	N
41171	Ab	12	0.062	5.63	0.35	8.1	N
41171	Ba	12	0.030	4.35	0.13	4.9	N
41171	Bb	12	0.017	3.80	0.07	3.1	N
49336	Aa	19	0.116	4.06	0.47	4.0	N
49336	Ab	19	0.082	5.96	0.49	8.8	N
49336	B	19	0.028	6.97	0.19	10.9	N
75663	Aa	19	0.218	6.85	1.50	10.7	Y
78163	Ba	12	0.355	4.26	1.51	4.6	N?
79979	Ba	5	0.194	4.30	0.83	4.7	Y
79979	Bb	5	0.115	3.71	0.43	2.7	N
103735	Aa	4	0.320	3.59	1.15	2.1	Y
103735	Ab	4	0.058	3.83	0.22	3.2	N
104440	Aa	3	0.274	5.03	1.38	6.7	Y
104440	Ab	3	0.025	4.96	0.13	6.5	N
103814	Aa	8	0.297	3.92	1.16	3.5	N
105879	Aa	1	0.193	5.69	1.10	6.9?	N
105879	Ab	1	0.045	3.19	0.14	1.0?	N
109443	Aa	6	0.266	4.97	1.32	6.5	Y
117666	Aa	10	0.209	3.81	0.80	3.1	N?
117666	Ba	10	0.194	3.69	0.71	2.6	N?

I use the long-term PMs determined by Brandt in place of the PMs measured by Gaia.

For some systems, spectroscopy is complemented by speckle interferometry of the outer pairs. Most speckle observations used here were made at the Southern Astrophysical Research Telescope (SOAR) and are referred to in the text simply as ‘SOAR data’. The latest observations and references to older publications are found in Tokovinin et al. (2022). Apart from the position measurements, speckle interferometry provides differential photometry of close visual pairs.

3. INDIVIDUAL OBJECTS

Figures in this section show the RV curves and the matching visual orbits for resolved subsystems. In the RV plots, green squares denote the primary component, blue triangles denote the secondary component, while the full and dashed lines plot the orbit. Typical error bars are smaller than the symbols. In the visual orbit plots, squares denote the measured positions, connected by short lines to the ephemeris positions on the orbital ellipse (solid line). Masses of stars are estimated from absolute magnitudes using standard main-sequence relations from Pecaut & Mamajek (2013). Orbital peri-

ods of wide pairs are evaluated statistically from their projected separations (see Tokovinin 2018a). Semimajor axes of spectroscopic subsystems are computed using the third Kepler’s law, and the photocenter amplitudes are evaluated based on the estimated masses and fluxes.

3.1. HIP 3645 (Triple)

This solar-type triple system belongs to the 67-pc sample. The outer 60'' common proper motion (CPM) pair A,B (LDS 9100) has been discovered by Luyten (1979). Star B is an M4V dwarf of $V = 15.2$ mag known as LP 646-9 with an accurate GDR3 parallax of 30.51 mas. The parallax of A is biased by the inner subsystem, first discovered as a 3.5 yr astrometric binary in Hipparcos (Goldin & Makarov 2007). This pair has been resolved in 2011 by Horch et al. (2017) at a separation of 30 mas (LSC 10 Aa,Ab). Its speckle monitoring at SOAR started in 2015. The three first observations did not resolve the pair, but the measurements in 2021 and 2022 are good, indicating a magnitude difference of $\Delta I = 1.1$ mag and a separation of up to 0''11.

Double lines were noted by Nordström et al. (2004), and the star is called ‘‘Spectroscopic binary’’ in Simbad. Most CHIRON spectra of A are also double-lined. The

Table 3. Spectroscopic Orbits

HIP	System	P	T	e	ω_A	K_1	K_2	γ	rms _{1,2}	$M_{1,2} \sin^3 i$
		(d)	(JD -2,400,000)		(deg)	(km s ⁻¹)	(km s ⁻¹)	(km s ⁻¹)	(km s ⁻¹)	(M_\odot)
3645	Aa,Ab	1529.6 ±3.7	59055.5 ±9.5	0.240 ±0.012	176.3 ±2.3	9.985 ±0.271	11.423 ±0.275	9.597 ±0.132	0.037 0.145	0.78 0.68
14313	Ba,Bb	6648.1 ±96.6	53347.9 ±105.7	0.488 ±0.008	318.1 ±1.5	8.048 ±0.153	8.228 ±0.155	21.540 ±0.049	0.184 0.191	1.01 0.99
36165	Aa,Ab	2300.4 ±16.1	57921.4 ±37.9	0.610 ±0.075	64.4 ±4.9	5.69 ±1.16	...	65.52 ±0.34	0.037 ...	1.28: 0.39
41171	Ba,Bb	963.1 ±1.7	58913.2 ±1.7	0.607 ±0.007	273.4 ±0.8	15.61 ±0.16	18.70 ±0.25	-3.32 ±0.07	0.30 0.46	1.10 0.92
41171	Aa,Ab	25.4133 ±0.0001	58449.999 ±0.005	0.5320 ±0.0005	308.25 ±0.09	47.18 ±0.23	48.27 ±0.03	-1.41 ±0.03	1.84 0.13	0.70 0.69
49336	Ba,Bb	1307.4 ±8.4	58895.8 ±38.4	0.163 ±0.021	132.5 ±11.4	4.55 ±0.15	...	-11.73 ±0.09	0.19 ...	1.35: 0.50
75663	Aa,Ab	623.76 ±0.21	59098.35 ±0.47	0.653 ±0.002	269.9 ±0.6	10.045 ±0.053	...	-56.352 ±0.029	0.041 ...	1.47: 0.48
78163	Ba,Bb	2083.2 ±20.4	59208.6 ±20.0	0.619 ±0.025	27.7 ±4.9	10.84 ±1.63	...	10.55 ±0.45	0.080 ...	0.93: 0.71
79979	Ba,Bb	1083.16 ±1.84	57635.32 ±4.81	0.610 ±0.003	349.8 ±1.3	15.31 ±0.16	18.01 ±0.21	0.00 ±0.06	0.121 0.204	1.14 0.97
103735	Aa,Ab	4251.8 ±12.1	59433.5 ±11.3	0.368 ±0.003	152.4 ±1.2	7.29 ±0.04	10.13 ±0.23	61.69 ±0.05	0.020 0.375	1.09 0.79
103814	Aa,Ab	1089.8 ±9.4	58393.5 ±16.1	0.601 ±0.079	331.0 ±9.1	4.48 ±1.44	...	-33.62 ±0.23	0.010 ...	1.78: 0.28
104440	A,B	1947.5 ±0.9	57909.2 ±1.7	0.631 ±0.002	178.5 ±0.8	10.202 ±0.044	16.759 ±0.180	-11.211 ±0.046	0.020 0.494	1.15 0.70
105879	Aa,Ab	2935.6 ±9.4	60032.2 ±13.0	0.631 ±0.019	359.7 ±2.5	11.07 ±0.66	13.83 ±0.91	35.44 ±0.14	0.418 0.843	1.24 1.00
109443	Aa,Ab	978.5 ±37.4	58715.3 ±210.9	0.214 ±0.084	24.3 ±67.7	3.02 ±0.34	...	-3.80 ±0.27	0.008 ...	1.30: 0.18
117666	Aa,Ab	781.2 ±1.6	59353.7 ±62.8	0.105 ±0.042	128.4 ±29.4	4.944 ±0.135	...	14.336 ±0.128	0.089 ...	0.97: 0.95:
117666	Ba,Bb	253.9 ±0.145	59204.8 ±2.5	0.269 ±0.018	113.9 ±3/3	9.28 ±0.16	...	14.264 ±0.132	0.128 ...	0.42 0.31

Table 4. Radial Velocities and Residuals (fragment)

HIP	System	Date	RV	σ	(O-C)	Comp.
HD		(JD -2,400,000)		(km s ⁻¹)		Instr.
3645	Aa,Ab	54781.5350	8.94	2.00	0.22	a
3645	Aa,Ab	57985.7810	13.38	0.50	0.05	a
3645	Aa,Ab	57985.7810	4.95	0.70	-0.40	b
3645	Aa,Ab	58130.5330	16.01	0.05	-0.01	a
3645	Aa,Ab	58130.5330	2.33	0.25	0.08	b

(This table is available in its entirety in machine-readable form). Instrument codes: B – Butler et al. (2017); E – Fiber echelle (Tokovinin 2015); F – Frasca et al. (2018) G – Gaia DR2; L – DuPont echelle (Tokovinin et al. 2015); N – Nidever et al. (2002)

RVs of Aa and Ab are used here jointly with the position measurements to derive a combined orbit (Figure 1). The period is 4.2 yr, longer than the Goldin’s one. The orbit is oriented edge-on, and the RV amplitudes trans-

late into Aa and Ab masses of 0.78 and 0.68 M_\odot , somewhat smaller than 0.94 and 0.80 M_\odot estimated from the absolute magnitudes. The visual orbit, unbiased parallax of B, and the spectroscopic mass ratio correspond to the masses of 0.97 and 0.85 M_\odot that agree better with the photometric estimates. The masses imply RV amplitudes 7% larger than measured, and this minor discrepancy could be caused by line blending. The ratio of dip areas corresponds to $\Delta m_{Aa,Ab} = 1.29$ mag, slightly larger than measured by speckle in the I band. Both components rotate slowly.

3.2. HIP 14307+14313 (Triple)

This system has some similarity to the previous one: a wide binary within 67 pc that hosts a subsystem. The 38'' pair A,B (DUN 10) has been known since 1826. The WDS lists another pair A,C at 510'' separation (TOK 428). Star C (HIP 14257, HD 19254, F7V) has a PM of (98.8, 67.6) mas s⁻¹, similar to the PMs of A and B, and for this reason it was listed in the survey

Table 5. Visual and Astrometric Orbits

HIP	System	P	T	e	a	Ω_A	ω_A	i
		(yr)	(yr)		(arcsec)	(deg)	(deg)	(deg)
3645	Aa,Ab	4.188 ± 0.010	2020.563 ± 0.026	0.240 ± 0.012	0.0967 ± 0.0014	314.0 ± 0.7	176.3 ± 1.7	97.6 ± 1.0
14313	Ba,Bb	18.20 ± 0.68	2004.94 ± 0.29	0.488 ± 0.008	0.1591 ± 0.0017	292.6 ± 0.3	318.1 ± 1.6	84.2 ± 0.5
49336	Ba,Bb	3.580 ± 0.023	2020.127 ± 0.105	0.163 ± 0.021	0.0071 ± 0.0009	9.3 ± 6.0	132.5 ± 11.4	140.4 ± 13.5
49336	A,B	397.8 ± 17.9	1971.24 ± 0.32	0.729 ± 0.010	0.886 ± 0.021	321.5 ± 1.6	253.5 ± 1.9	142.3 ± 1.5
79979	Ba,Bb	2.966 ± 0.005	2016.674 ± 0.013	0.610 ± 0.003	0.0601 ± 0.0007	103.8 ± 0.7	349.8 ± 1.3	82.9 ± 1.0
103735	Aa,Ab	11.64 ± 0.03	2021.598 ± 0.031	0.368 ± 0.003	0.1363 ± 0.0009	168.1 ± 0.4	152.4 ± 1.2	87.4 ± 0.7
104440	A,B	5.332 ± 0.003	2017.424 ± 0.005	0.631 ± 0.002	0.1905 ± 0.0013	194.3 ± 0.4	178.5 ± 0.8	93.0 ± 1.0
105879	Aa,Ab	8.037 ± 0.026	2023.237 ± 0.036	0.631 ± 0.019	0.0669 ± 0.0018	231.5 ± 1.0	359.7 ± 2.5	97.0 ± 1.6
117666	Aa,Ab	2.138 ± 0.004	2021.33 ± 0.17	0.105 ± 0.043	0.0079 ± 0.0007	26.1 ± 5.3	128.4 ± 29.4	148.0 fixed
117666	A,B	30.073 ± 0.071	2020.392 ± 0.044	0.309 ± 0.004	0.1809 ± 0.0009	24.3 ± 1.4	356.5 ± 1.5	147.5 fixed

Table 6. Radial Velocities of Other Components

HIP	Comp.	Date	RV
		(JD -2,400,000)	(km s ⁻¹)
14257	C	57986.8700	28.496
36160	B	56940.8450	64.859
36160	B	57266.9055	64.884
36160	B	58121.7557	64.889
36160	B	58193.5556	64.881
36160	B	58546.5656	64.873
36160	B	59168.7635	64.899
105879	D	55477.5014	36.077
105879	D	56885.7159	35.714

of CPM pairs (Tokovinin & Lépine 2012). However, the difference of the PM, parallax (14.70 mas according to GDR3), and RV (28.5 km s⁻¹, see Table 6) of star C with respect to A and B rule out its physical association. There is no excessive astrometric noise in A and C (RUWE close to 1) in GDR3, and no parallax for B because it is a close binary.

Star B has been resolved by speckle interferometry at SOAR in 2014 and bears the name TOK 428 Ba,Bb in the WDS. The pair slowly opened up from 0".19 to 0".21 by 2016, closed down to 33 mas in 2021.96, and was resolved again in 2022.68 after passing through the conjunction. Double lines in the CHIRON spectra show

only a slow evolution, as can be seen in the RV curve (Figure 2). The preliminary combined 18 yr orbit fitted to the RVs and position measurements predicts periastron in 2023 March, when the largest RV difference between Ba and Bb will occur. Continued observations are needed to improve our first orbit.

Speckle interferometry at SOAR established the magnitude difference of $\Delta I_{\text{Ba,Bb}} = 0.42 \pm 0.06$ mag, while the ratio of dip areas gives $\Delta m_{\text{Ba,Bb}} = 0.19$ mag. The latter leads to the visual magnitudes of 9.25 and 9.44 for Ba and Bb, respectively, and the “photometric” masses of 0.90 and 0.87 M_{\odot} . The “spectroscopic” masses are slightly larger, 1.01 and 0.99 M_{\odot} , and the orbital parallax of 18.26 mas matches well the GDR3 parallax of A, 18.36 mas. Stars Ba and Bb rotate slowly and have no lithium line.

3.3. HIP 36165+36160 (Triple)

The wide 17" pair of HIP 36165 (star A, $V = 7.03$ mag, F6V) and HIP 36160 (star B, $V = 8.19$ mag, G1.5V) has been discovered by John Herschel in 1835 (HJ 3969). The fast and common PM, matching parallaxes and RVs prove the bound nature of this pair with an estimated period of 15 kyr. Nordström et al. (2004) noted that the RVs of both A and B were variable. However, CHIRON and other sources indicate that B has a constant RV of 64.9 km s⁻¹ and is most likely a single star (RUWE 1.0 in GDR3). The RV of A, on the other hand, varies with a small amplitude; this motion

Table 7. Positional Measurements and Residuals

HIP	System	T	θ	ρ	σ	O-C $_{\theta}$	O-C $_{\rho}$
		(yr)	($^{\circ}$)	($''$)	($''$)	($^{\circ}$)	($''$)
3645	Aa,Ab	2011.6850	159.8	0.0300	0.002	5.4	0.000
3645	Aa,Ab	2011.9417	139.9	0.0598	0.002	-0.1	-0.000
3645	Aa,Ab	2014.7537	311.2	0.1076	0.002	0.3	-0.000
3645	Aa,Ab	2021.8909	320.5	0.0742	0.002	-1.9	-0.001
3645	Aa,Ab	2022.4447	316.3	0.1153	0.002	0.2	0.000
14313	Ba,Bb	2014.7635	107.9	0.1911	0.002	-0.4	0.001
14313	Ba,Bb	2014.7635	108.3	0.1908	0.002	-0.0	0.000

(This table is available in its entirety in machine-readable form)

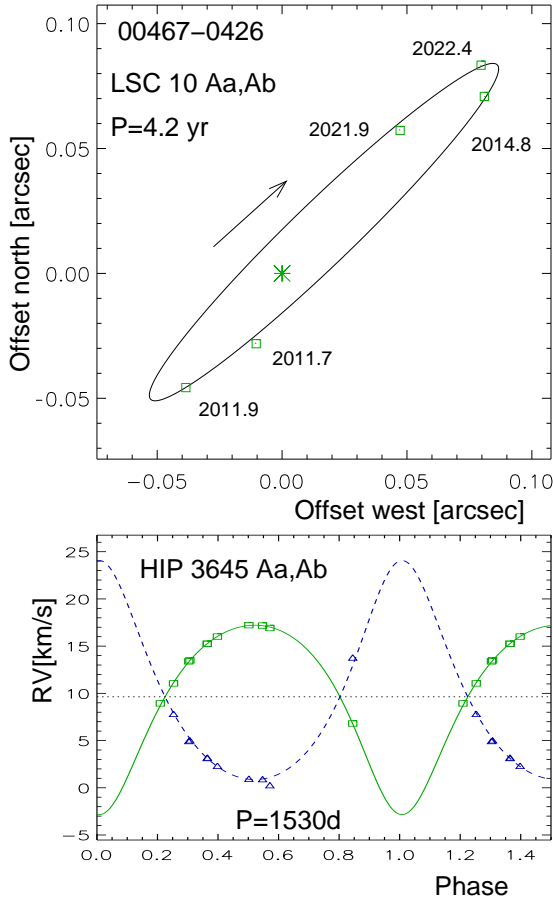


Figure 1. Visual orbit and RV curve of HIP 3645 Aa,Ab.

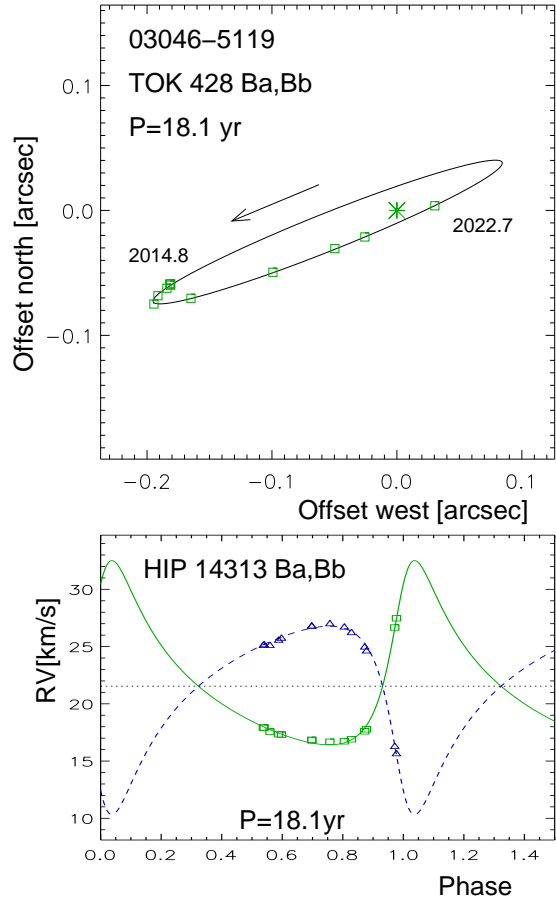


Figure 2. Visual orbit and RV curve of HIP 14313 Ba, Bb.

produces astrometric noise in Gaia (RUWE 11.9) and a large acceleration detected by Brandt (2021).

The spectroscopic orbit with a period of 6.3 yr derived from the CHIRON RVs is illustrated in Figure 3. The descending part of the RV curve is not yet covered, so the orbit is preliminary. The period is well constrained, but the eccentricity can be larger. The estimated mass of Aa, $1.28 M_{\odot}$, matches its spectral type F6V. The minimum mass of Ab is $0.39 M_{\odot}$; no spectral lines of Ab are

detectable, while speckle and adaptive optics imaging (Tokovinin et al. 2010) has not resolved any subsystems around stars A and B.

3.4. HIP 41171 (Quadruple)

This is a rare case of a quadruple-lined object (SB4). The system has been presented and discussed in paper 6 of this series (Tokovinin 2019), where a 25-day SB2 orbit of Aa,Ab (main component in the 0 $^{\prime}$.9 visual pair

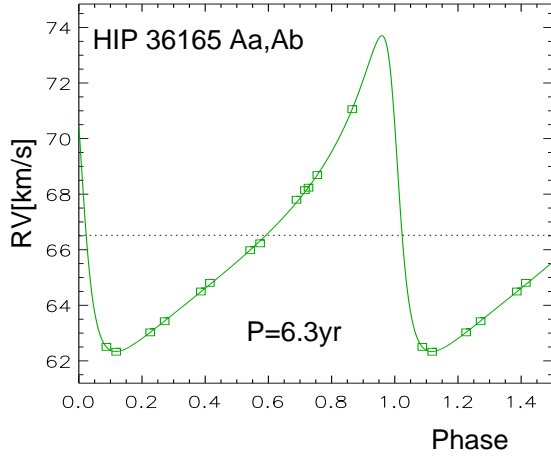


Figure 3. The RV curve of HIP 36165 Aa,Ab.

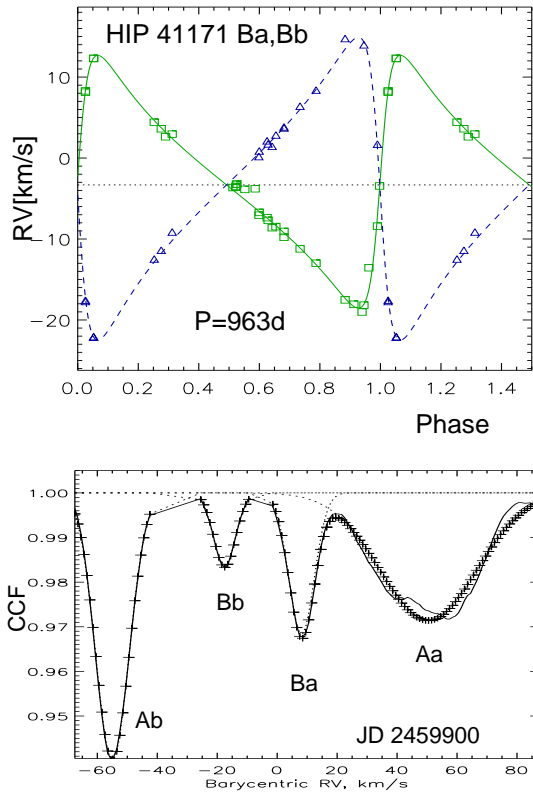


Figure 4. The RV curve of HIP 41171 Ba,Bb (top) and the CCF with four well-separated dips recorded on JD 2,459,900 (bottom, solid line). The plus signs show the sum of four Gaussian curves, plotted individually by dotted lines.

RST 4396) was determined. The lines of Ba and Bb are clearly separated from the lines of Aa and Ab only in certain phases of the 25-day orbit. Systematic monitoring at these moments during several years has led eventually to the determination of the 2.6 yr orbit of Ba,Bb (Figure 4). The RVs of Aa and Ab match the published

orbit; slightly refined elements of Aa,Ab derived with additional data are given in Table 3.

The visual magnitudes of Ba and Bb (10.95 and 11.38 mag, respectively) were estimated from the areas of the four CCF dips. They correspond to the masses of 1.09 and $1.00 M_{\odot}$ (mass ratio $q_{\text{Ba,Bb}} = 0.92$), similar to the spectroscopic masses $M \sin^3 i$ of 1.10 and $0.92 M_{\odot}$ ($q_{\text{Ba,Bb}} = 0.83$). This means that the orbit of Ba,Bb has a large inclination. It is oriented unfavorably ($\omega = 273^{\circ}$), so despite the estimated semi-major axis of 12mas the pair Ba,Bb has never been resolved by speckle interferometry at SOAR, not even partially, in 9 visits. The prospect of its resolution with larger telescopes or interferometers is good, though. The outer pair A,B has an estimated period of 1.2 kyr and moves very slowly in retrograde sense. It has covered a 22° arc since its discovery in 1940. The 0'9 pair is recognized as two sources in GDR3, which gives a parallax of 4.93 ± 0.03 mas (RUWE 1.6) for A and no parallax for B.

3.5. HIP 49336 (Quadruple)

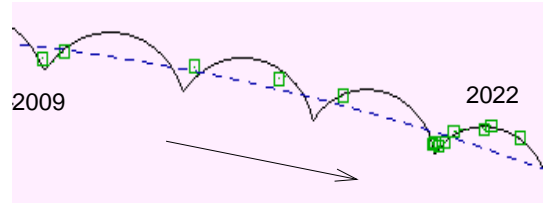
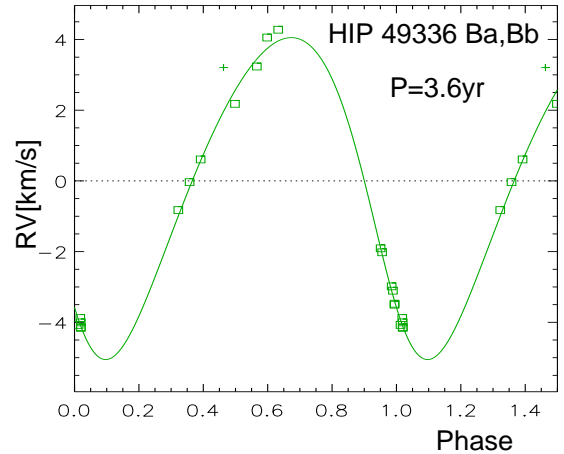


Figure 5. The RV curve of HIP 49336 Ba,Bb (top, the plus sign marks uncertain measurement) and a fragment of the outer orbit with wobble (bottom). The black solid and blue dashed lines represent the outer orbit with and without wobble, respectively. The green squares are the measured positions of B relative to A.

Like the previous object, this quadruple system is a left-over from the previous work (paper 7, Tokovinin

2020), where the 44.5-day orbit of the main subsystem Aa,Ab was established. The outer pair I 292 (ADS 7629) has a visual orbit with $P = 380$ yr and $a = 0''.869$. It is not resolved by CHIRON, and the spectra are triple-lined. The lines of Ba, free from blending when the lines of Aa and Ab are well separated, show a slow RV variation detected in paper 7. Monitoring with CHIRON at favorable phases of Aa,Ab has continued for a few more years (with an interrupt for COVID-19) and now the orbit of Ba,Bb with a period of 3.6 yr is sufficiently well constrained.

When the existence of a long-period subsystem was established, more frequent speckle observations at SOAR were scheduled in hope of detecting the wobble. Indeed, as shown in the lower panel of Figure 5, the apparent motion of A,B deviates from the smooth blue line describing the outer orbit. The elements of A,B and Ba,Bb were fitted jointly with ORBIT3 using both position measurements and RVs. This helps to better constrain the period of Ba,Bb and defines the orientation of its orbit. The RV difference between A and B identifies the correct ascending node of the outer orbit and the mutual inclination, 33° . The small eccentricity $e_{\text{Ba,Bb}} = 0.16$ indicates absence of the Lidov-Kozai cycles, in agreement with moderate mutual inclination.

The inclination of Ba,Bb determined from the wobble and the RV amplitude lead to the Bb mass of $0.50 M_\odot$, assuming that Ba is a $1.35 M_\odot$ star. The resulting mass ratio $q_{\text{Ba,Bb}} = 0.37$ and the semimajor axis of 31.4 mas imply a wobble with an amplitude of 8.5 mas, similar to 7.1 mas found from fitting the A,B positions.

3.6. HIP 75663 (Quadruple)

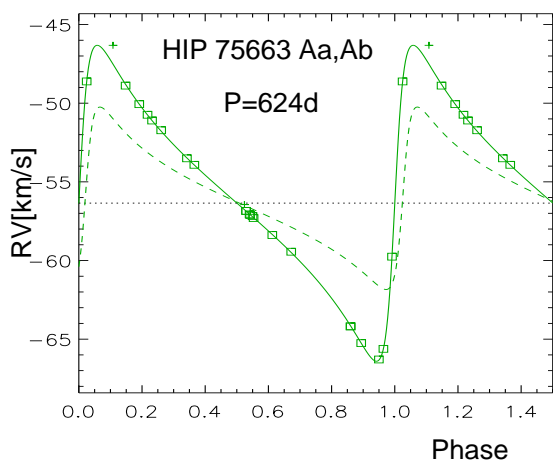


Figure 6. The RV curve of HIP 75663 Aa,Ab. Dashed line is the RV curve of the GDR3 orbit with corrected ω .

Components A and B of the $9''.4$ visual binary STF 1939 (ADS 9640) are resolved by the CHIRON $2''.7$

fiber aperture, so their RVs are measured separately. As established in paper 4 (Tokovinin 2018b), star B is a double-lined twin binary with a period of 22.9 days and $e_{\text{Ba,Bb}} = 0.61$, while the RV of A varies with a long period. Continued CHIRON monitoring leads to an orbital period of 623.8 days (1.7 yr), see Figure 6. The periastron in 2020.68 was missed because of the telescope closure to COVID-19, but the following periastron of this eccentric ($e_{\text{Aa,Ab}} = 0.65$) orbit in 2022.39 has been well covered. I also used six RVs from Butler et al. (2017) with an offset of -56.85 km s^{-1} chosen to fit the orbit (the published RVs have arbitrary zero point).

Gaia DR3 independently determined a spectroastrometric orbit of HIP 75663A with a period of 626.6758 days and amplitude $K_1 = 5.80 \text{ km s}^{-1}$. The general character of this orbit is similar to the one presented here, although the argument of periastron $\omega = 94^\circ.5$ is inverted. The dashed line in Figure 6 shows the GDR3 orbit with ω corrected by 180° . Fitting an astrometric orbit removes the bias of parallax and PM, leading to a good agreement between parallaxes of A (7.73 mas) and B (7.78 mas); the biased parallax of A in GDR3 is 8.97 mas with a RUWE of 5.45. Note that the short period of Ba,Bb and the equality of its components make its GDR3 astrometry bias-free (RUWE 1.05).

As noted in paper 4, star A is located slightly above the main sequence (estimated age ~ 4 Gyr), and the lithium line is detectable in the spectra of both A and B. The Aa mass of $1.47 M_\odot$ estimated from the standard relation for dwarfs is only approximate. The corresponding minimum mass of Ab derived from our orbit is $0.48 M_\odot$. If the orbital inclination of $69^\circ.1$ measured by Gaia is adopted, the mass of Ab becomes $0.52 M_\odot$. On the other hand, the Ab mass derived from the GDR3 astrometric orbit is $0.46 M_\odot$, less than the minimum spectroscopic mass, while the small RV amplitude in the GDR3 orbit leads to a minimum mass of $0.09 M_\odot$. The actual mass of Ab should therefore be close to $0.5 M_\odot$ and the semimajor axis of the Aa,Ab orbit is 14 mas.

3.7. HIP 78163 (Quadruple)

The 2+2 quadruplet HIP 78163 resembles the previous one, but with inverted roles of the components. The double-lined twin pair Aa,Ab with $P = 21.8$ days and $e_{\text{Aa,Ab}} = 0.58$ is very similar to star B in HIP 75663 (22.9 days, $e = 0.61$); its orbit has been determined in paper 4 of this series (Tokovinin 2018b). Star B of HIP 78163 is located at $5''.9$ from A (WG 185 pair in the WDS, estimated period 7.4 kyr). The RV of B varies slowly, and, as for the previous object, Gaia determined an orbit with a period of 1532 days, this time only an astrometric one. The period found here is longer, 2083 days (5.7

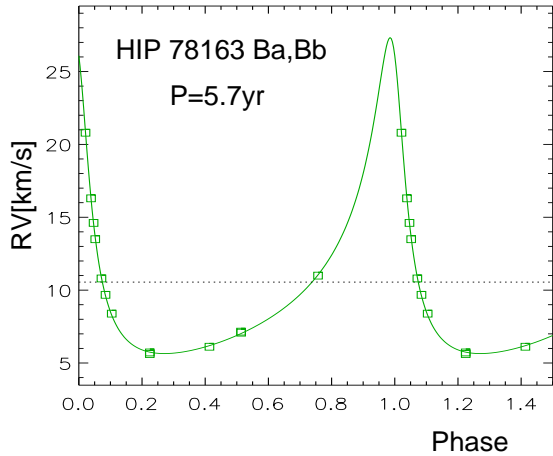


Figure 7. The RV curve of HIP 78163 Ba,Bb.

yr). The Gaia astrometric orbital fit gives a parallax of 10.65 mas for B which agrees much better with the 10.49 mas parallax of A (unbiased, RUWE 0.86). In contrast, the raw (biased, RUWE 6.22) GDR3 parallax of B is 11.28 mas, while DR2 measured an even more discrepant parallax of 13.57 mas. The duration of the GDR3 mission is only 34 months, so a more accurate orbit of Ba,Bb is expected in the future releases.

The spectroscopic orbit of Ba,Bb shown in Figure 7 is eccentric, $e_{\text{Ba,Bb}} = 0.62$. The RV maximum is not fully covered, but the next periastron is expected only in 2026. I use with a low weight the RV measured in 2015.5 by Gaia because the CHIRON data cover only 1690 days. Adopting a mass of $0.93 M_{\odot}$ for Ba, the minimum mass of Bb is $0.71 M_{\odot}$. Lines of Bb might be detectable in the spectra, unless it is a white dwarf. However, the spectra can be partially contaminated by the light of A, depending on the seeing and guiding (the separation is only $5''.9$), so accurate modeling of the CCFs needed to extract the RVs of Bb is problematic.

3.8. HIP 79979+79980 (Triple)

The outer $23''.4$ pair A,B (BSO 12) has been known since 1837. Its brighter component A ($V = 5.51$ mag, F5IV) is listed in the bright star catalog as HR 6077. The fainter ($V = 6.82$ mag, F9V) star B has its own designations HIP 79979 and HD 146835. The RV variability of B was suspected by Nordström et al. (2004). The RVs of A and B were found equal in (Tokovinin et al. 2015), casting doubt on the existence of a subsystem, but the first CHIRON spectrum taken in 2017 produced a double CCF. By that time, B has been resolved at SOAR as a tight visual pair TOK 410. The preliminary orbit with $P = 3$ yr predicted periastron in 2022.6, as actually observed (Figure 8).

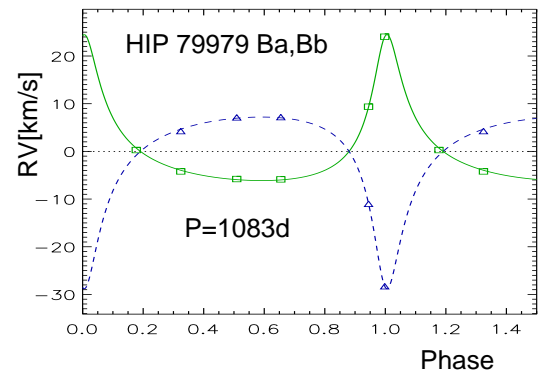
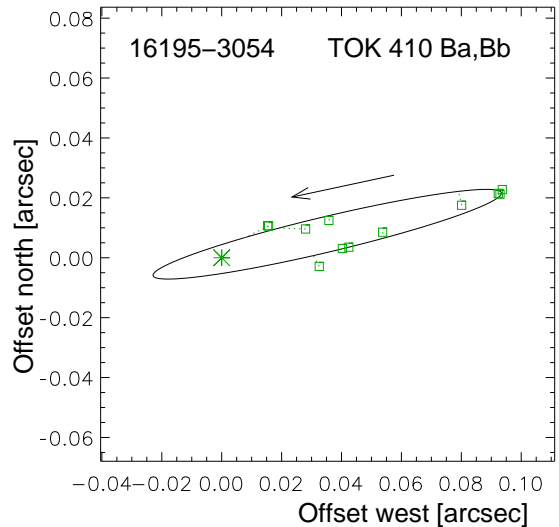


Figure 8. Visual orbit and RV curve of HIP 79979 Ba,Bb.

Using the unbiased parallax of 22.71 mas measured in GDR3 for A, the Ba,Bb orbit gives the mass sum of $2.11 M_{\odot}$. This matches the spectroscopic masses of 1.14 and $0.97 M_{\odot}$ (the inclination $i_{\text{Ba,Bb}} = 82^{\circ}.9$ is known) and the absolute magnitudes of Ba and Bb. So, despite the modest number of RVs, the orbit of Ba,Bb is reasonably well defined.

Stars A and B have almost identical $V - K$ colors (see table 1), but differ by 1.3 mag in the V band. Star A is obviously evolved; it is located above the main sequence. In contrast, star B, despite being a binary, is located on the standard main sequence.

3.9. HIP 103735 (Triple)

The primary component A ($V = 7.66$ mag, G3V) of the wide $186''$ pair is a visual and spectroscopic binary. The secondary star B (2MASS J21012669-3509333, $V = 17.14$ mag) is a white dwarf identified by Tokovinin & Lépine (2012) in the large PM survey and confirmed by Gaia.

Both Nidever et al. (2002) and Nordström et al. (2004) noted that RV of A was variable. The first CHIRON spectrum taken in 2017 revealed an asymmetric

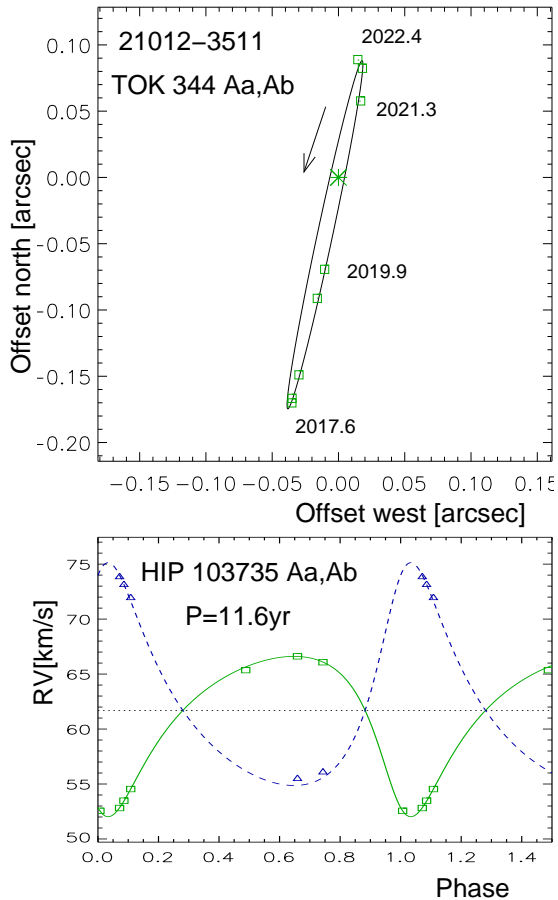


Figure 9. Visual orbit and RV curve of HIP 103735 Aa,Ab.

(blended) CCF. The same year the $0''.14$ pair Aa,Ab has been resolved at SOAR (TOK 344 Aa,Ab). In the following five years, the pair passed through the periastron: the separation decreased and increased again, the CCF dips separated apart. These data allow calculation of a combined orbit with $P = 11.6$ yr presented in Figure 9. One RV published by Nidever et al. (2002) is used, it refers to the brighter star Aa.

The combined orbit yields masses of 1.00 and $0.72 M_{\odot}$ for Aa and Ab, respectively, and an orbital parallax of 21.5 mas, in rough agreement with the accurate GDR3 parallax of star B, 22.09 mas. The GDR3 parallax of A is inaccurate and biased, 23.55 ± 0.47 mas. The astrometric acceleration is reflected by the large RUWE of 15.6 , as well as by the PM anomaly (Brandt 2021).

3.10. HIP 103814 (Triple)

The $57''$ pair of bright stars HIP 103814 (HR 8042, $V = 6.64$ mag, G3IV+K0IV) and HIP 103839 ($V = 6.90$ mag, K0III) has been known since 1826 (DUN 236 in the WDS). B is redder than A and brighter in the K band.

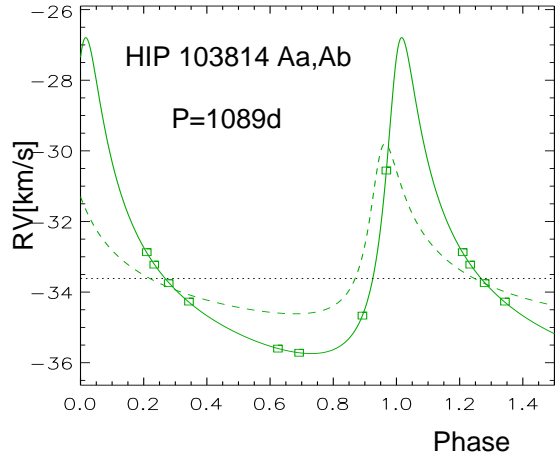


Figure 10. RV curve of HIP 103814 Aa,Ab. The GDR3 orbit is traced by the dashed line.

This is a rare pair composed of two giants, and it does not belong to the 67-pc sample of solar-type stars.

The fact that star A is a binary follows from its astrometric acceleration detected by Hipparcos, RUWE of 23.0 in GDR3, and, possibly, composite spectrum. The eight CHIRON RVs do not fully constrain the orbit shown in Figure 10. However, the GDR3 spectroastrometric orbit with $P = 1119.65$ days confirms the period independently. The shape of the Gaia RV curve is similar (after correcting ω by 180°), although its amplitude is substantially smaller (2.41 km s^{-1}) compared to the CHIRON orbit (4.48 km s^{-1}).

Assuming that the mass of Aa is $1.78 M_{\odot}$, the GDR3 astrometric orbit with an amplitude of 7.7 mas corresponds to the Ab mass of $0.53 M_{\odot}$ (the full semimajor axis is 33.3 mas). This implies a early-M dwarf companion which contributes negligible light, so the spectrum of A cannot be composite. The minimum Ab mass derived from the CHIRON orbit is $0.28 M_{\odot}$, and the actual mass is $0.62 M_{\odot}$, considering the inclination of the astrometric orbit. The width and contrast of the CCF dip do not change with orbital phase, proving that Ab is much fainter than Aa.

3.11. HIP 104440 (Triple)

This is a resolved visual triple located at 20 pc from the Sun (GJ 818.1). The outer $6''.4$ pair AB,C has been known since 1894 (HDO 305). Star C is faint ($V = 13.5$ mag) and red, likely an M4V dwarf. AB,C is in slow retrograde motion with an estimated period of 1 kyr. The PM difference between AB and C is caused by motion in the outer orbit.

The bright ($V = 5.68$ mag, F9.5V) visual pair A,B known as I 379 has been presumably discovered by R. Innes in 1898, although we know now that the separations on the order of $1''$ measured by him were totally

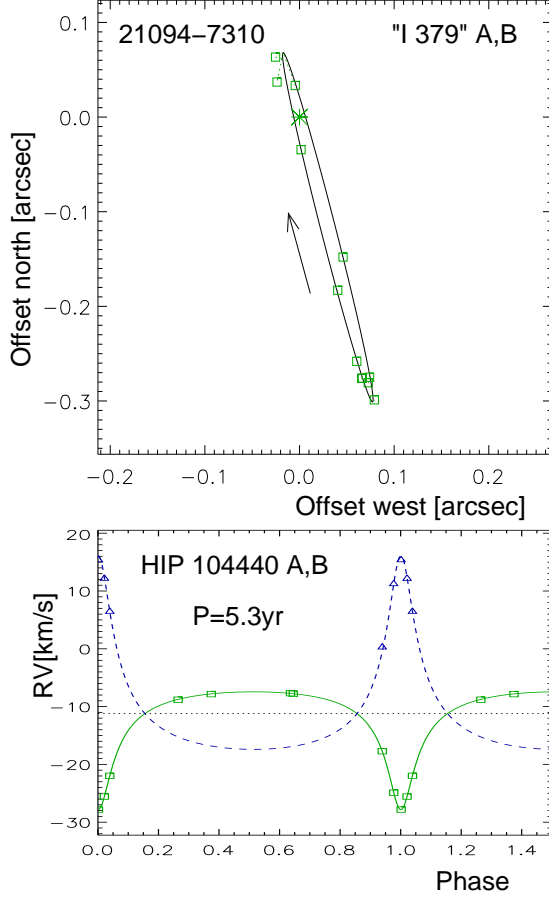


Figure 11. Visual orbit and RV curve of HIP 104440 A,B.

wrong (this pair is never wider than $0''.3$). Apart from the three spurious measurements by Innes, only W. Finzen reported a resolution of this pair in 1932 which also does not match the orbit. The magnitude difference measured at SOAR is substantial, $\Delta y = 3.15$ mag, and such close pairs are beyond the capacity of visual observers. In this case, the WDS name I 379 corresponds to the spurious discovery, despite several “confirming” visual resolutions.

Goldin & Makarov (2007) published two possible astrometric orbits of this star with periods of 6.65 and 5.87 yr based on Hipparcos transits. The true period is even shorter, 5.3 yr. The first visual orbit of A,B which also used the CHIRON RVs has been published in (Tokovinin et al. 2020); it is updated here (Figure 11). The pair goes through the periastron in 2022.9, and the previous periastron in 2017.4 has been also covered. The orbit ignores spurious historic micrometer measurements and is based entirely on the SOAR and CHIRON data.

The absolute magnitudes of A and B correspond to the masses of 1.13 and 0.72 M_{\odot} and a dynamic parallax of 49.7 mas which compares well with the GDR3 parallax

of star C, 50.6 mas; the GRD3 parallax of A, 47.0 mas, is biased. Masses derived from the combined orbit are 1.15 and 0.74 M_{\odot} , and the orbital parallax is 51.0 mas.

3.12. HIP 105879 (Triple)

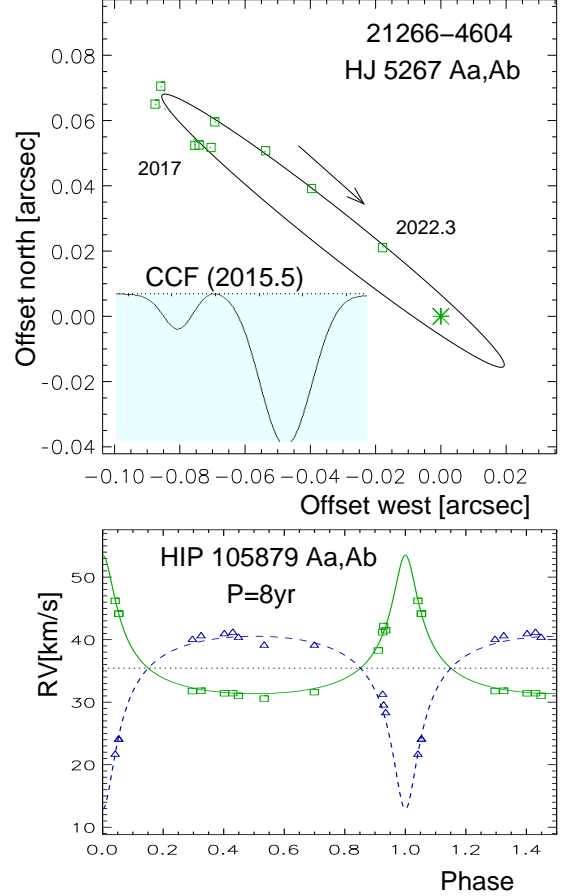


Figure 12. Visual orbit and RV curve of HIP 105879 Aa,Ab. The insert shows the CCF recorded on JD 2457218 when the dips were well separated.

This is yet another typical solar-type triple system composed of wide and tight visual pairs. Star A ($V = 7.18$ mag, F7V) has been identified as a double-lined binary with CHIRON in 2015.5, first resolved at SOAR in 2017.6, and designated in the WDS as HJ 5267 Aa,Ab. The variable RV was noted previously by Nordström et al. (2004), astrometric acceleration was detected by Hipparcos and by its comparison with Gaia. The wide companion D (CD-46 13953, $V = 9.96$ mag) at $44''$ has a matching PM and RV. Its GDR3 parallax of 13.102 ± 0.014 mas defines accurate distance to the system. The companion B, seen only once by J. Herschel in 1834 at $5''$, is spurious, and the companion C at $238''$ listed in the WDS is optical. So, to the best of our knowledge, this is a triple system.

The combined orbit of Aa,Ab with $P = 8.0$ yr and a substantial eccentricity $e_{\text{Aa,Ab}} = 0.63$ is presented in Figure 12. The first spectrum has been taken in 2010.8 using fiber echelle (Tokovinin 2015), and the 11.9 yr coverage defines the orbital period quite well. The pair Aa,Ab goes through periastron in 2023.2, when it will not be visible behind the Sun. Unfortunately, the period is an integer number of years and in the foreseeable future all periastrons will occur during poor visibility periods. The pair was unresolved at SOAR in 2015.74 and in 2022.68 in agreement with the orbit that predicted small separations on those dates.

The CCF dips are well separated only near the periastron, as illustrated in the Figure. In other phases they are blended, and the fits of two overlapping Gaussians are less reliable. The ratio of the dip areas when they are well separated corresponds to the magnitude difference of 2.21 mag, in agreement with the differential photometry at SOAR ($\Delta y = 2.14$ mag, $\Delta I = 1.94$ mag). This relatively large magnitude difference does not match the moderate spectroscopic mass ratio $q_{\text{Aa,Ab}} = 0.80$. The mass ratio and the mass sum of $2.06 M_{\odot}$ derived from the visual elements and the parallax of star D lead to the individual masses of 1.14 and $0.92 M_{\odot}$ for Aa and Ab, respectively, while the absolute magnitude of Aa corresponds to a mass of $1.5 M_{\odot}$ on the main sequence. In fact, A is elevated above the main sequence by ~ 1 mag, so Aa starts to evolve into a subgiant. This explains the apparent discrepancy between mass ratio and magnitude difference in the inner pair. The spectroscopic mass sum is $2.2 M_{\odot}$, suggesting that the RV amplitudes might be slightly over-estimated.

Star D has not been resolved by speckle interferometry at SOAR, it has low astrometric noise in Gaia and an apparently constant RV that matches the RV of A. So, it is unlikely that D has close companions.

3.13. HIP 109443 (Triple)

The bright solar-type star HIP 109443 ($V = 7.63$ mag, F8V) is an astrometric binary detected by Hipparcos and confirmed both by Brandt (2021) and by a RUWE of 10.3 in GDR3. A survey of astrometric binaries with the NICI AO instrument detected a faint companion B at $1''.4$ separation (Tokovinin et al. 2012, TOK 216). The estimated period of ~ 700 yr makes it unlikely that the acceleration and variable RV (Nordström et al. 2004) are caused by this companion.

Nine CHIRON spectra show the RV variability, and the GDR3 spectroscopic orbit matches these RVs quite well (Figure 13). The fit of 6 elements to 9 RVs is almost perfect, leaving rms residuals of only 0.008 km s^{-1} .

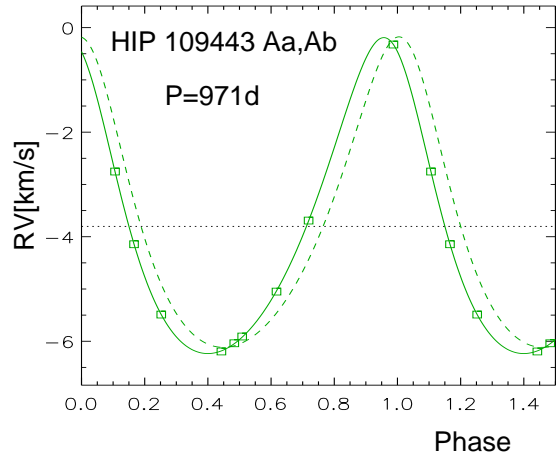


Figure 13. RV curve of HIP 109443 Aa,Ab. The dashed line is the Gaia spectroscopic orbit.

The minimum mass of Ab is $0.18 M_{\odot}$ if the mass of Aa is $1.3 M_{\odot}$. The large RUWE indicates clear detection of the astrometric signal, but, for some reason, GDR3 determined only the spectroscopic orbit, leaving the inclination and the true mass of Ab unconstrained. The mass of B is about $0.56 M_{\odot}$, as inferred from its K -band luminosity. It is detected by Gaia at $1''.4129$ ($\Delta G_{\text{A,B}} = 4.85$ mag), showing little motion since 2011. The parallax of B measured by GDR3, 15.58 mas, is close to the parallax of A in GDR2 (15.33 mas), but GDR3 gives a biased parallax of 12.74 mas for A. The bias will be removed when the astrometric orbit of Aa,Ab is determined by Gaia.

3.14. HIP 117666 (Quadruple)

This 9th magnitude star (HD 2236888, G5V) appeared to be a normal tight visual binary, first resolved by R. Aitken in 1913 (A 2700, ADS 17052, WDS J23518–0637). The visual orbit with a 30 yr period, last updated by Docobo & Ling (2009), is very well constrained. It is fully covered by accurate speckle measurements (the first one in 1985) and is rated grade 2 in the orbit catalog.

The star attracted attention as an X-ray source and for this reason four high-resolution spectra were taken by Frasca et al. (2018) in 2001. Double lines were detected in one spectrum, suggesting presence of a subsystem. Double lines were also seen in the spectrum taken by Tokovinin (2015) in 2010. This prompted further monitoring with CHIRON. It was not clear from the outset whether double lines were produced by motion in the visual orbit or by an inner subsystem. The first CHIRON spectrum taken in 2017.6 looked single-lined, but in 2019.6 the lines were double again, so I started regular monitoring. The first seven CHIRON CCFs are shown in Figure 14, illustrating blending of two components

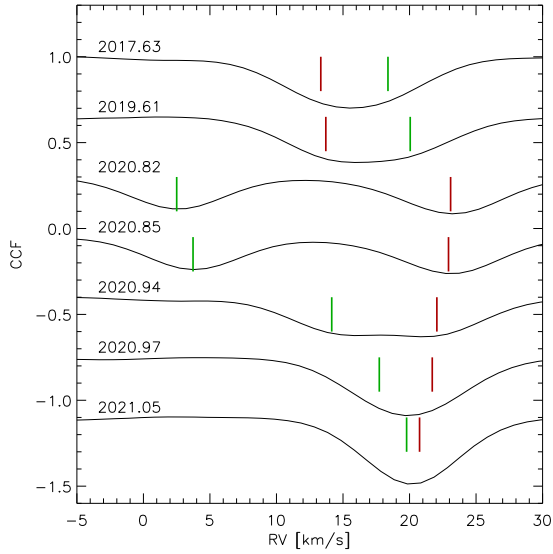


Figure 14. CCFs of the first 7 CHIRON spectra of HIP 117666. The curves are displaced vertically by 0.35 to avoid overlap. The dates are indicated. Thick red and green lines mark the RVs of Aa and Ba, respectively, according to the orbits.

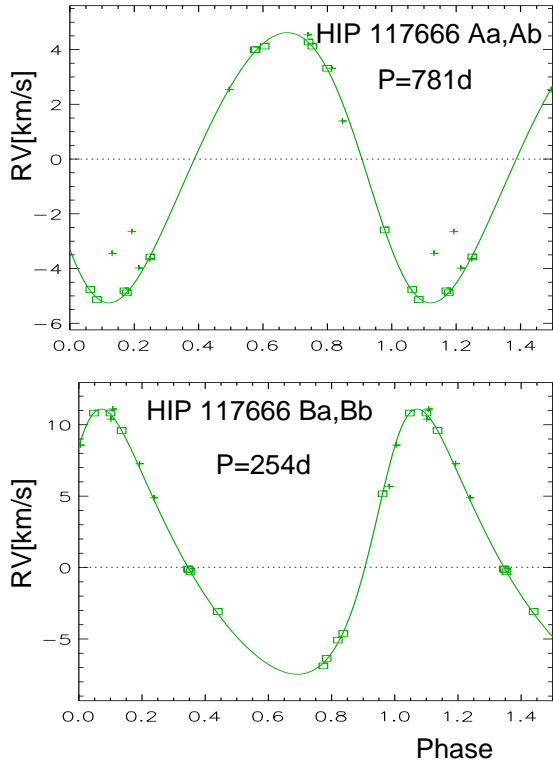


Figure 15. RV curves of the subsystems Aa,Ab and Ba,Bb in HIP 117666. Squares mark the RVs derived from double CCFs, plus signs correspond to blended CCFs. Motion in the outer orbit is subtracted.

with independent RV variation. The RVs of both CCF

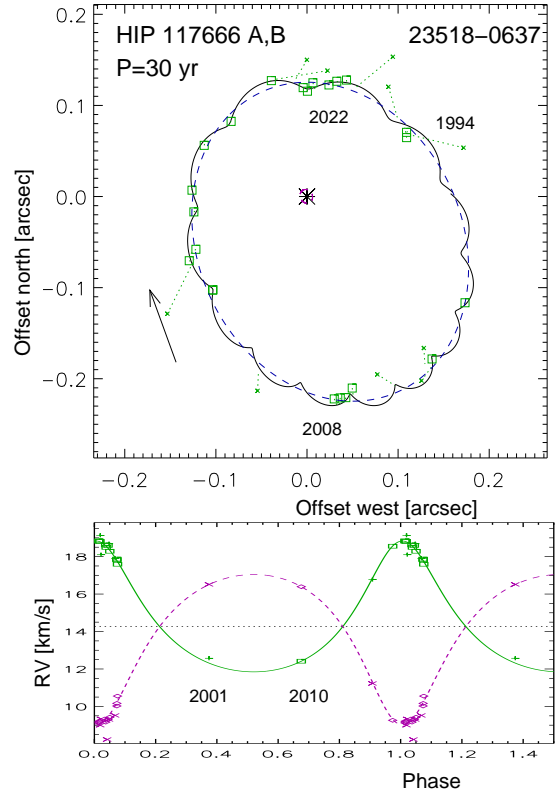


Figure 16. Outer orbit of HIP 117666 A,B on the sky (top) and the RV curve where motion in the inner subsystems is subtracted (bottom).

dips vary faster than prescribed by the visual orbit, so this system is actually a 2+2 quadruple.

Five RVs of HIP 117666 averaging at ~ -1 km s $^{-1}$ were reported by Tokovinin & Smekhov (2002). They are not compatible with the orbits presented here. It turns out that these RVs refer to another 9th magnitude star, HD 223695 (F6IV), which is located at 1' east of HIP 117666 and has an RV of -2.3 km s $^{-1}$ according to Simbad. Somehow, the visual binary was misidentified, and the spectral type of F6V quoted in the above paper (instead of G5V) confirms this suspicion. One of the RVs reported by Frasca et al. (JD 24 52209.43) also apparently refers to HD 223695. Proximity of two stars on the sky means that the X-ray source can be actually associated with HD 223695 (with a fast rotation of 22.0 km s $^{-1}$ according to Frasca et al.), rather than with the slowly rotating components of the HIP 117666 system. The Galactic velocity of HIP 117666, $U, V, W = (-23.8, -10.1, -21.3)$ km s $^{-1}$, does not match any known kinematic group, and the lithium line in its spectrum is not detectable, so this star is not young.

Deciphering the two inner orbits from the often-blended CCFs with similar dips, superposed on the slow

RV variation due to the outer orbit, was a challenging task, addressed iteratively. First, the faster variation of the smaller dip Ba was matched to a period of ~ 250 days, then the RVs of Aa yielded a period of 2 yr with a different systemic velocity. A model was constructed to represent the blended dips by the outer and two inner orbits using the dip amplitudes and widths measured in the well-resolved phases. Comparison of all CCFs to this model inspired confidence in the adopted inner periods.

The available tool, `ORBIT3`, does not allow for simultaneous fit of all three orbits. After several iterations on the orbits of A,B and Aa,Ab, the RVs of Ba were corrected for the motion in the outer orbit and fitted as a single-lined binary. Then the motion of Ba,Bb was subtracted from the RVs of Ba, and a joint fit of the remaining inner orbit Aa,Ab and the outer orbit A,B was done using `ORBIT3`, including the speckle measurements. The astrometric elements of Aa,Ab (wobble) were also determined. The rms residuals of accurate SOAR speckle positions without wobble, 6 mas, are reduced to 2 mas when the wobble is fitted. The smaller wobble caused by the Ba,Bb motion is left unmodeled. In the orbital fit, I used the RVs measured in 2002 by Frasca et al. with a small weight and a correction of $+1 \text{ km s}^{-1}$.

Speckle interferometry at SOAR establishes the magnitude difference $\Delta m_{A,B} = 0.14 \text{ mag}$ (WDS quotes 0.2 mag), so the individual V magnitudes of A and B are 9.41 and 9.55 mag, respectively. The Gaia DR2 parallax of $13.4 \pm 1.3 \text{ mas}$ is inaccurate and potentially biased, GDR3 gives no parallax, so I adopt the dynamical parallax of 13.2 mas that follows from the good-quality outer orbit and the estimated masses. Neglecting the light of the secondaries Ab and Bb, the masses of Aa and Ba matching their absolute magnitudes are 0.98 and $0.97 M_{\odot}$; they agree with the combined spectral type G5V and the $V - K$ color. The mass of Ab deduced from the RV amplitude and inclination (see below) is $0.45 M_{\odot}$, the minimum mass of Bb is $0.31 M_{\odot}$. Small masses of the inner secondaries explain why their lines are not visible in the spectra. The estimated system mass is therefore $2.70 M_{\odot}$.

The estimated masses, periods, and parallax yield the semimajor axes of the inner orbits, 25.1 and 11.2 mas. The ratio of the measured photo-center amplitude of Aa,Ab, 7.9 mas, to the semimajor axis equals the wobble factor $f_{Aa,Ab} = q_{Aa,Ab}/(1 + q_{Aa,Ab}) = 0.31$, hence the mass ratio is $q_{Aa,Ab} = 0.46$ and the estimated mass of Ab is $0.45 M_{\odot}$. The astrometric orbit of Aa,Ab yields a loosely constrained inclination $i_{Aa,Ab} = 141^{\circ} \pm 13^{\circ}$. The inner inclination of $i_{Aa,Ab} = 143^{\circ}$ matches the Ab mass estimated from the wobble, so I fixed this value. The minimum mass of Bb leads to an estimated wobble

amplitude of 2 mas for Ba. This unmodeled (so far) wobble contributes to the residuals of accurate speckle positions.

As noted, the outer orbit (Figure 16) is very well constrained. However, the fitted inclination of $i_{A,B} = 149^{\circ}6 \pm 1^{\circ}5$ and the RV amplitudes of 3.42 and 4.15 km s^{-1} lead to the outer mass sum of $3.25 M_{\odot}$, substantially larger than the estimated $2.7 M_{\odot}$ and in disagreement with the absolute magnitudes and spectral type. This discrepancy is removed by fixing the outer inclination to a slightly smaller value of $147^{\circ}5$. So, the inclinations of both Aa,Ab and A,B are fine-tuned (within limits allowed by the data) to reach consistency between all orbital parameters and the estimated masses. The nodal angles Ω in both orbits are similar, hence Aa,Ab and A,B have well aligned orbits. If the orbit of Ba,Bb were also coplanar with A,B, the mass of Bb would be $0.55 M_{\odot}$, making B more massive than A. This contradicts the measured outer mass ratio $q_{A,B} = 0.82$. The inclination $i_{Ba,Bb}$ could be close to 110° in order to avoid the Lidov-Kozai oscillations (the eccentricity of Ba,Bb is only 0.27).

The architecture of this remarkable quadruple and its internal dynamics deserve further investigation. The period ratio $P_{A,B}/P_{Aa,Ab} = 14.05$ is small, so the orbits interact dynamically and the motion is more complex than the simple superposition of Keplerian orbits fitted here; our orbits represent osculating elements in the current epoch. Furthermore, the ratio of two inner periods $P_{Aa,Ab}/P_{Ba,Bb} \approx 3$ is close to an integer number. The two inner orbits could be trapped into a 1:14:42 mean motion resonance with the outer orbit.

4. SUMMARY

The original goal of this project has been inspired by the lack of known orbital elements for inner subsystems revealed previously by variable RV or astrometric acceleration. Periods and mass ratios inferred from the orbits are necessary for a statistical study of nearby hierarchies. However, our RV monitoring has shown that some hierarchies, believed to be triple, are in fact 2+2 quadruples, as both visual components have variable RVs. Orbits of the short-period subsystems in these quadruples have been quickly determined and reported in the first papers of this series. Observation of other components with slow RV variation continued for several years, eventually yielding their spectroscopic orbits as well. Four such “returning clients” from the previous papers are presented here: HIP 41171, 49336, 75663, and 78163. In the first two, the outer pairs are sub-arcsecond, so the spectra of all visible stars are blended. Recovering RVs of slowly varying subsystems from blended spec-

tra dominated by fast RV variation of other pairs required careful planning of observations at phases where the blending is minimized.

HIP 117666 is another tricky quadruple studied here. It is a well-known visual binary where existence of an inner subsystem has been suggested but remained unproven. Unexpectedly, our observations discovered that both visual components contain subsystems. Patient accumulation of blended spectra was needed to decipher the underlying orbits, including the outer one. A similar case (HIP 12548) has been presented in paper 8.

The perturbing effects of binaries on the astrometry were anticipated in the design of the Gaia mission, and GDR3 delivered a large set of orbits which reduce biases in the astrometric solutions. However, complexity of some triple and quadruple hierarchies precludes their modeling by the Gaia pipeline. Only dedicated monitoring with adequate cadence, time coverage, and spectral resolution can reveal the true nature of systems like HIP 12548 and 117666. Even relatively easy cases of spectroscopic subsystems in well-resolved visual pairs (HIP 75663A, 79163B, and 103814A) demonstrate that some Gaia orbits can be inaccurate or even wrong. Gaia is an outstanding astrometric facility which has not been designed to deal with complex hierarchies.

Long orbital periods of subsystems studied here favor their direct resolution. Six combined orbits based on CHIRON RVs and speckle-interferometric measurements at SOAR were determined. Another two are added from modeling wobble in the motion of their rel-

atively close outer pairs. Spatial resolution (or wobble detection) complements spectroscopic orbits, allowing to measure masses and to deduce orbit orientation. The latter is particularly valuable when orientation of the outer orbit is also known. Architecture of hierarchical systems (mutual orbit orientation, periods and masses) contains information on their still debated origin.

I thank operators of the 1.5-m telescope for executing observations of this program and the SMARTS team for scheduling and pipeline processing.

The research was funded by the NSF's NOIR-Lab. This work used the SIMBAD service operated by Centre des Données Stellaires (Strasbourg, France), bibliographic references from the Astrophysics Data System maintained by SAO/NASA, and the Washington Double Star Catalog maintained at USNO. This work has made use of data from the European Space Agency (ESA) mission *Gaia* (<https://www.cosmos.esa.int/gaia>), processed by the *Gaia* Data Processing and Analysis Consortium (DPAC, <https://www.cosmos.esa.int/web/gaia/dpac/consortium>). Funding for the DPAC has been provided by national institutions, in particular the institutions participating in the *Gaia* Multilateral Agreement. This research has made use of the services of the ESO Science Archive Facility.

Facility: CTIO:1.5m, SOAR, Gaia

REFERENCES

- Brandt, T. D. 2021, *ApJS*, 254, 42, doi: [10.3847/1538-4365/abf93c](https://doi.org/10.3847/1538-4365/abf93c)
- Butler, R. P., Vogt, S. S., Laughlin, G., et al. 2017, *AJ*, 153, 208, doi: [10.3847/1538-3881/aa66ca](https://doi.org/10.3847/1538-3881/aa66ca)
- Docobo, J. A., & Ling, J. F. 2009, *AJ*, 138, 1159, doi: [10.1088/0004-6256/138/4/1159](https://doi.org/10.1088/0004-6256/138/4/1159)
- Frasca, A., Guillout, P., Klutsch, A., et al. 2018, *A&A*, 612, A96, doi: [10.1051/0004-6361/201732028](https://doi.org/10.1051/0004-6361/201732028)
- Gaia Collaboration, Brown, A. G. A., Vallenari, A., et al. 2021, *A&A*, 649, A1, doi: [10.1051/0004-6361/202039657](https://doi.org/10.1051/0004-6361/202039657)
- Gaia Collaboration, Arenou, F., Babusiaux, C., et al. 2022, arXiv e-prints, arXiv:2206.05595, <https://arxiv.org/abs/2206.05595>
- Goldin, A., & Makarov, V. V. 2007, *ApJS*, 173, 137, doi: [10.1086/520513](https://doi.org/10.1086/520513)
- Horch, E. P., Casetti-Dinescu, D. I., Camarata, M. A., et al. 2017, *AJ*, 153, 212, doi: [10.3847/1538-3881/aa6749](https://doi.org/10.3847/1538-3881/aa6749)
- Luyten, W. J. 1979, NLTT catalogue. Volume_I. +90_to_+30_ Volume_II. +30_to_0_
- Mason, B. D., Wycoff, G. L., Hartkopf, W. I., Douglass, G. G., & Worley, C. E. 2001, *AJ*, 122, 3466, doi: [10.1086/323920](https://doi.org/10.1086/323920)
- Nidever, D. L., Marcy, G. W., Butler, R. P., Fischer, D. A., & Vogt, S. S. 2002, *ApJS*, 141, 503, doi: [10.1086/340570](https://doi.org/10.1086/340570)
- Nordström, B., Mayor, M., Andersen, J., et al. 2004, *A&A*, 418, 989, doi: [10.1051/0004-6361:20035959](https://doi.org/10.1051/0004-6361:20035959)
- Paredes, L. A., Henry, T. J., Quinn, S. N., et al. 2021, *AJ*, 162, 176, doi: [10.3847/1538-3881/ac082a](https://doi.org/10.3847/1538-3881/ac082a)
- Pecaut, M. J., & Mamajek, E. E. 2013, *ApJS*, 208, 9, doi: [10.1088/0067-0049/208/1/9](https://doi.org/10.1088/0067-0049/208/1/9)
- Tokovinin, A. 2014, *AJ*, 147, 87, doi: [10.1088/0004-6256/147/4/87](https://doi.org/10.1088/0004-6256/147/4/87)
- . 2015, *AJ*, 150, 177, doi: [10.1088/0004-6256/150/6/177](https://doi.org/10.1088/0004-6256/150/6/177)
- . 2016a, *AJ*, 152, 11, doi: [10.3847/0004-6256/152/1/11](https://doi.org/10.3847/0004-6256/152/1/11)

- . 2016b, Orbit: IDL Software For Visual, Spectroscopic, And Combined Orbits, Zenodo, doi: [10.5281/zenodo.61119](https://doi.org/10.5281/zenodo.61119)
- . 2017, ORBIT3: Orbits of Triple Stars, Zenodo, doi: [10.5281/zenodo.321854](https://doi.org/10.5281/zenodo.321854)
- . 2018a, ApJS, 235, 6, doi: [10.3847/1538-4365/aaa1a5](https://doi.org/10.3847/1538-4365/aaa1a5)
- . 2018b, AJ, 156, 194, doi: [10.3847/1538-3881/aadfe6](https://doi.org/10.3847/1538-3881/aadfe6)
- . 2019, AJ, 158, 222, doi: [10.3847/1538-3881/ab4c94](https://doi.org/10.3847/1538-3881/ab4c94)
- . 2020, AJ, 160, 69, doi: [10.3847/1538-3881/ab9b1e](https://doi.org/10.3847/1538-3881/ab9b1e)
- . 2022, AJ, 163, 161, doi: [10.3847/1538-3881/ac5330](https://doi.org/10.3847/1538-3881/ac5330)
- Tokovinin, A., Fischer, D. A., Bonati, M., et al. 2013, PASP, 125, 1336, doi: [10.1086/674012](https://doi.org/10.1086/674012)
- Tokovinin, A., Hartung, M., & Hayward, T. L. 2010, AJ, 140, 510, doi: [10.1088/0004-6256/140/2/510](https://doi.org/10.1088/0004-6256/140/2/510)
- Tokovinin, A., Hartung, M., Hayward, T. L., & Makarov, V. V. 2012, AJ, 144, 7, doi: [10.1088/0004-6256/144/1/7](https://doi.org/10.1088/0004-6256/144/1/7)
- Tokovinin, A., & Latham, D. W. 2017, ApJ, 838, 54, doi: [10.3847/1538-4357/aa6331](https://doi.org/10.3847/1538-4357/aa6331)
- Tokovinin, A., & Lépine, S. 2012, AJ, 144, 102, doi: [10.1088/0004-6256/144/4/102](https://doi.org/10.1088/0004-6256/144/4/102)
- Tokovinin, A., Mason, B. D., Mendez, R. A., & Costa, E. 2022, AJ, 164, 58, doi: [10.3847/1538-3881/ac78e7](https://doi.org/10.3847/1538-3881/ac78e7)
- Tokovinin, A., Mason, B. D., Mendez, R. A., Costa, E., & Horch, E. P. 2020, AJ, 160, 7, doi: [10.3847/1538-3881/ab91c1](https://doi.org/10.3847/1538-3881/ab91c1)
- Tokovinin, A., Pribulla, T., & Fischer, D. 2015, AJ, 149, 8, doi: [10.1088/0004-6256/149/1/8](https://doi.org/10.1088/0004-6256/149/1/8)
- Tokovinin, A. A., & Smekhov, M. G. 2002, A&A, 382, 118, doi: [10.1051/0004-6361:20011586](https://doi.org/10.1051/0004-6361:20011586)